Geophysical Research Letters®

Key Points:
- The pattern of sea-surface temperature changes affects clear-sky longwave radiative cooling, and thus hydrological sensitivity
- Different tropical warming patterns explain differences in hydrological sensitivity between uniform warming and coupled experiments

Sea-Surface Temperature Patterns, Radiative Cooling, and Hydrological Sensitivity

Andrew I. L. Williams[1,2] ![ORCID] and Nadir Jeevanjee[3] ![ORCID]

[1]Program in Atmospheric and Oceanic Sciences, Princeton University, Princeton, NJ, USA, [2]Scripps Institution of Oceanography, University of California San Diego, San Diego, CA, USA, [3]Geophysical Fluid Dynamics Laboratory, Princeton, NJ, USA

Abstract Global climate models project an increase in global-mean precipitation in response to increases in global-mean surface temperature; that is, a positive "hydrological sensitivity." However, there are hints in the literature that global-mean precipitation is sensitive to the *pattern* of warming in addition to global-mean warming. Here we leverage previous theoretical insights into tropical dynamics and radiative cooling to connect clear-sky longwave radiative cooling, a key component of hydrological sensitivity, to sea-surface temperature (SST) patterns in the tropics. We use this theory to explain why hydrological sensitivity is about 25% larger in uniform warming scenarios compared to abrupt-4xCO2 runs. This discrepancy is driven by different changes in clear-sky longwave radiative cooling in the tropics, which we quantitatively attribute to differences in the rate of SST warming in regions of tropical convection.
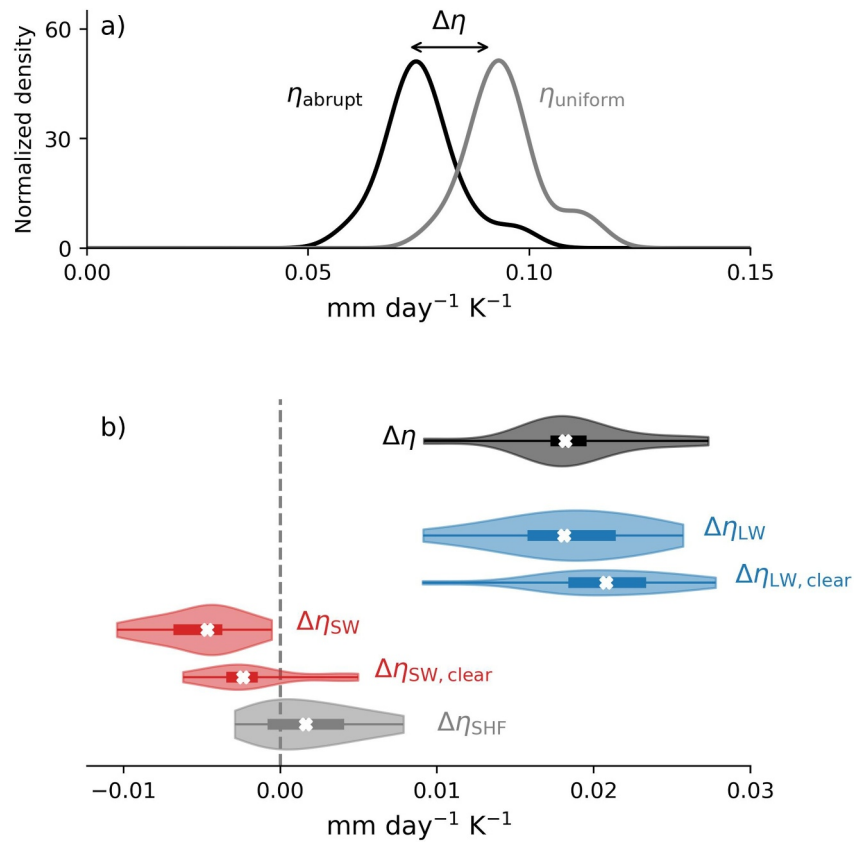
Plain Language Summary When climate scientists want to understand how the total amount of rainfall on Earth will change as the planet warms, they can use two types of computer simulations: one where ocean temperatures are warmed uniformly everywhere, and another where CO_2 is rapidly increased and the climate warms up in response. We show that the uniform warming experiments consistently predict about 25% more rainfall increase per degree of warming. The reason lies in where the warming occurs—uniform experiments heat up the rainy, stormy regions of the tropics just as much as everywhere else, while the natural response experiments tend to warm the dry Eastern tropical Pacific more than the rainy Western Pacific (similar to El Niño patterns). Since tropical thunderstorms are the atmosphere's main way of communicating temperature changes throughout the troposphere, warming the stormy regions more effectively warms the atmosphere and increases its ability to cool itself through radiation to space. To maintain energy balance, this enhanced cooling must be matched by more rainfall. This research helps explain why different experimental setups can give different predictions for future precipitation, and highlights that changes in the water cycle depend on not just how much warming occurs, but *where* that warming occurs.

1. Introduction

Since the earliest general circulation model studies it has been noted that global-mean precipitation increases in response to increases in global-mean surface temperature (Manabe & Wetherald, 1975). Given this observation, it is common to define the "hydrological sensitivity," η, which measures the rate of change of global-mean precipitation with respect to global-mean surface temperature. Global-mean precipitation is also affected by atmospheric "adjustments" to climate forcers such as CO_2 or black carbon, but η just measures the surface temperature-mediated component of global-mean precipitation change.

The reason for the increase in precipitation with surface warming is that, in the global-mean and in steady-state, latent heating of the atmosphere (through precipitation) must be balanced by atmospheric cooling, which is primarily achieved through longwave cooling to space (Methods) (Allen & Ingram, 2002; Pendergrass & Hartmann, 2014). To explain this increase in longwave cooling to space, Jeevanjee and Romps (2018) (hereafter, JR18) introduced a theory which relates changes in clear-sky radiative cooling to changes in the "temperature depth" of the troposphere. We will revisit their argument in Section 5, but for now we note that the theory of JR18 provides a physical theory for what sets the order-of-magnitude of radiative cooling changes (and hence η) under warming.

While relating global-mean precipitation to global-mean temperature has been illuminating, there are a few cases in the literature which suggest η is sensitive to the *pattern* of sea-surface temperature (SST) warming in addition to

Figure 1. *Hydrological sensitivity is systematically larger in uniform warming* versus *abrupt-4xCO₂ simulations, due to longwave clear-sky cooling.* (a) Kernel density estimates of η calculated in uniform warming and abrupt-4xCO₂ simulations; kernel density estimates are computed using the `gaussian_kde` function from SciPy (Virtanen et al., 2020). (b) Violin plots of the difference in hydrological sensitivity ($\Delta\eta$) between uniform warming and abrupt-4xCO₂ simulations, with decomposition in contributions from longwave cooling ($\Delta\eta_{LW}$), shortwave cooling ($\Delta\eta_{SW}$), and sensible heat fluxes ($\Delta\eta_{SHF}$). Also shown are the contributions from clear-sky longwave cooling ($\Delta\eta_{LW,\ clear}$) and shortwave cooling ($\Delta\eta_{SW,\ clear}$). Distributions show the minimum and maximum changes; the median change plotted with a cross and the boxes show the inter-quartile range of changes.

its global-mean value. For example, Zhao and Knutson (2024) found that η was roughly 35% larger in atmosphere-only experiments where the imposed pattern of SST warming resembled the observed SST trend over recent decades compared to when the pattern was taken from the historical run of a coupled climate model. Similarly, S. Zhang et al. (2023) used "patch warming" SST experiments with CAM5 to show that η was larger in response to SST warming in regions of tropical ascent compared to warming in other regions of the globe.

This potential dependence of η on SST patterns has also arisen in the context of different warming scenarios explored as part of the Coupled Model Intercomparison Project (CMIP). Specifically, in addition to the abrupt-4xCO₂ experiment in a fully coupled model, many centers also ran uniform warming experiments with an atmosphere-only model. It is possible to calculate η using both of these setups (Fläschner et al., 2016), yielding two estimates of η. Interestingly, Fläschner et al. (2016) noted that, in the multi-model mean, η is *larger* when estimated using uncoupled, uniform-warming experiments than when estimated using fully coupled abrupt-4xCO₂ simulations (see also Figure 1a). We denote this difference between the η estimated using uniform warming simulations and abrupt-4xCO₂ simulations as

$$\Delta\eta \equiv \eta_{uniform} - \eta_{abrupt}. \tag{1}$$

One obvious difference between uniform warming and abrupt-4xCO₂ simulations is the CO₂ levels. Enhanced CO₂ levels somewhat weaken hydrological sensitivity through spectral masking (Cohen & Pincus, 2025), but we

find that this is only able to explain a small fraction of the magnitude of $\Delta\eta$ across models (Figure S1 in Supporting Information S1).

Beyond CO_2 levels, another difference between uniform warming and abrupt-4xCO$_2$ simulations is that abrupt-4xCO$_2$ simulations exhibit *patterned* SST warming. For example, abrupt-4xCO$_2$ simulations tend to warm more in the Eastern tropical Pacific than the Western tropical Pacific (sometimes called an "El Niño-like" warming pattern). So, could differences in SST warming patterns explain the difference between η_{uniform} and η_{abrupt} across models? The literature is divided on this question. Fläschner et al. (2016) argue that patterned SST warming is *not* the reason for higher mean η in uniform warming simulations, whereas a recent paper by S. Zhang et al. (2023) suggested that SST warming patterns were in fact a driver of the positive $\Delta\eta$ in models. However, S. Zhang et al. (2023) do not provide a quantitative theory which links patterns of SST warming to differences in hydrological sensitivity.

The literature thus raises a couple of questions: "Does hydrological sensitivity depend on the pattern of SST warming?" and, if so, "What mechanisms cause this?" Furthermore, do these mechanisms arise from existing theories for hydrological sensitivity, or do they represent entirely different physics?

Give these questions, our goal in this paper is to quantify the link between SST patterns, radiative cooling, and η, with an eye toward explaining the positive $\Delta\eta$ across models in terms of their differing SST patterns. We begin by demonstrating that $\Delta\eta$ is in fact *systematically* positive across CMIP models, that is, that every CMIP model has $\eta_{\text{uniform}} > \eta_{\text{abrupt}}$. We then decompose $\Delta\eta$ into contributions from changes in sensible heat fluxes and longwave/shortwave radiative cooling using the global-mean atmospheric energy budget (Equation 2). We then leverage theoretical insights from Fueglistaler et al. (2015) and Jeevanjee and Romps (2018) to *quantitatively* link different patterns of SST warming to changes in clear-sky radiative cooling and hydrological sensitivity. We conclude by arguing that the systematically positive $\Delta\eta$ across models is because uniform warming simulations have stronger warming in regions of tropical deep convection than abrupt-4xCO$_2$ simulations, leading to greater free-tropospheric warming and increases in radiative cooling per degree of global-warming. We then discuss how our theory can explain recent results in the literature related to SST warming patterns and hydrological sensitivity.

2. Methods

2.1. CMIP Simulations

We use an ensemble of simulations from the CMIP, Phases 5 and 6. We use all models for which all data was available for the abrupt-4xCO$_2$, AMIP, and AMIP-p4K simulations. We used monthly mean data to calculate all quantities, but down-sampled all timeseries to yearly frequency before calculating regressions to minimize the influence of serial autocorrelation on our statistics.

We used 15 models in total, 8 from CMIP5 and 7 from CMIP6. We choose to combine CMIP5 and CMIP6 together throughout the paper to increase the sample size, but our conclusions are unchanged if we restrict ourselves to simply using a single generation of models. A full list of the models used is provided in Supporting Information S1.

2.2. Global-Mean Energetic Decomposition

Changes in precipitation with warming can be understood using the steady-state, global-mean atmospheric energy budget (Pendergrass & Hartmann, 2014). This states that the net heating of the atmosphere through latent heat release and surface sensible heat flux must be balanced by the net radiative cooling of the atmosphere, which can be split into longwave and shortwave components (Mitchell et al., 1987; O'Gorman et al., 2012). When considering climate perturbations, denoted by δ, we arrive at the following expression,

$$L\delta P + \delta\text{SHF} = \delta Q_{\text{LW}} + \delta Q_{\text{SW}},\tag{2}$$

where L is the latent heat of condensation of water vapor, P is the precipitation rate, SHF is the upwards sensible heat flux at the surface, and Q_{LW} and Q_{SW} are the longwave and shortwave radiative cooling, respectively. Equation 2 can be rearranged to express changes in precipitation in terms of changes in sensible heat flux and radiative cooling.

All of the terms on the right-hand side of Equation 2 are initially calculated in energy units (Wm^{-2}), before being transformed into "precipitation units" ($mm\ day^{-1}$).

2.3. Hydrological Sensitivity Calculations

η measures the surface temperature-mediated component of global-mean precipitation change, and we estimate this in two ways. The difference between the AMIP-p4K and AMIP simulations is used to calculate $\eta_{uniform}$, and a regression approach is used to calculate η_{abrupt} in the abrupt-4xCO$_2$ simulations (DeAngelis et al., 2015; Fläschner et al., 2016). To estimate η_{abrupt}, we calculate a least squares regression of global-mean precipitation against global-mean near-surface air temperature for years 0–140 of the abrupt-4xCO$_2$ scenario. Our conclusions are unchanged if we use the Theil-Sen estimator (which is more robust to outliers) instead of ordinary least squares regression. Our conclusions regarding $\Delta\eta$ are also unaffected if we instead use years 20–140 of the abrupt-4xCO$_2$ scenario to estimate η_{abrupt}, though the precise value of η_{abrupt} is slightly sensitive to the choice of time period.

Through the energy budget (Equation 2) we can decompose hydrological sensitivity (η) into contributions from longwave cooling, shortwave cooling, and sensible heat fluxes,

$$\eta = \eta_{LW} + \eta_{SW} + \eta_{SHF,} \tag{3}$$

where we have absorbed the minus sign in the sensible heat flux term from Equation 2 so that a positive η_{SHF} indicates a *reduction* in upwards surface sensible heat flux.

We calculate each of these terms by regression of their respective global-mean components against global-mean near-surface air temperature, as for η. We also decompose the longwave cooling and shortwave cooling terms into their all-sky and clear-sky components.

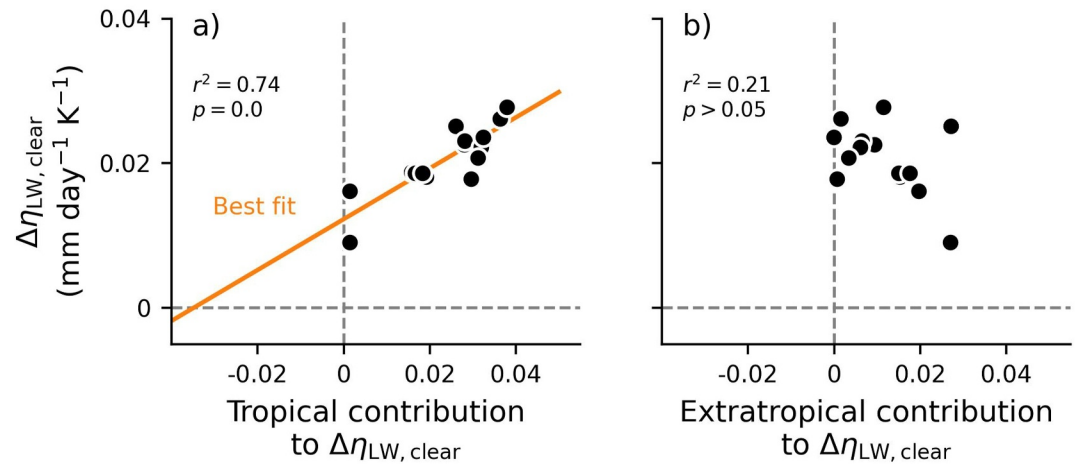## 3. Changes in η Are Driven by Longwave, Clear-Sky Cooling

We begin by demonstrating that η calculated using uniform warming simulations is in fact larger than η calculated from abrupt-4xCO$_2$ simulations, and that this is a common feature across models. This is a step beyond the results of Fläschner et al. (2016), who only showed that $\eta_{uniform} > \eta_{abrupt}$ holds in the multi-model mean.

Figure 1a shows probability density functions of η derived from both uniform warming and abrupt-4xCO$_2$ simulations. Visually, it is apparent that $\eta_{uniform} > \eta_{abrupt}$ in the multi-model mean. To assess whether this holds on a model-by-model basis, Figure 1b shows violin plots of the difference in η between uniform warming experiments and abrupt-4xCO$_2$ simulations (denoted as $\Delta\eta$). We find that η is systematically larger in uniform warming experiments compared to the abrupt-4xCO$_2$ coupled runs—that is, a positive $\Delta\eta$—with a median difference of around $\Delta\eta \approx 0.02\ mm\ day^{-1}\ K^{-1}$. In fractional terms, this means that $\eta_{uniform}$ is on average about 25% larger than η_{abrupt} in CMIP models.

In Figure 1b we also show the contributions to $\Delta\eta$ from longwave cooling $\left(\Delta\eta_{LW}\right)$, shortwave cooling $\left(\Delta\eta_{SW}\right)$ and upwards sensible heat fluxes at the surface $\left(\Delta\eta_{SHF}\right)$. We also show the contribution from changes in clear-sky longwave cooling $\left(\Delta\eta_{LW,\ clear}\right)$ and shortwave cooling $\left(\Delta\eta_{SW,\ clear}\right)$. The larger hydrological sensitivity in uniform warming versus abrupt-4xCO$_2$ runs is mostly due to differences in clear-sky longwave cooling, while changes in sensible heat flux and clear-sky shortwave cooling are similar between the uniform warming and abrupt-4xCO$_2$ runs.

4. Differences in $\Delta\eta_{LW,\ clear}$ Are Driven by the Tropics

We will now argue that $\Delta\eta_{LW,clear}$ is primarily driven by *tropical* changes in longwave, clear-sky cooling per degree of global warming, as opposed to being associated with radiative changes in the extratropics. This is illustrated in Figure 2, which shows scatter plots of $\Delta\eta_{LW,clear}$ against its contributions from tropical and extratropical radiative cooling. The tropical contribution to $\Delta\eta_{LW,clear}$ is calculated as $\Delta(d\langle Q_{LW,clear}\rangle/dT_s)$ where $\langle\cdot\rangle$ indicates an area-weighted tropical average ($\pm30°$ of the equator) and Δ denotes the difference between a quantity calculated using uniform warming and abrupt-4xCO$_2$ experiments. The extratropical contribution is calculated

Figure 2. *Differences in longwave clear-sky cooling between uniform and abrupt-*4xCO$_2$ *experiments are driven by changes in the tropics*. (a) Scatterplot of $\Delta\eta_{\text{LW,clear}}$ against the contribution from tropical changes in longwave, clear-sky cooling. (b) Scatterplot of $\Delta\eta_{\text{LW,clear}}$ against the contribution from extratropical changes in longwave, clear-sky cooling.

similarly but we average the longwave, clear-sky cooling over all points poleward of $\pm 30°$. Note that in order to keep things neat, in the bulk of the paper we will denote the tropical contribution to $\Delta\eta_{\text{LW,clear}}$ as $\Delta\langle\eta_{\text{LW,clear}}\rangle$.

$\Delta\eta_{\text{LW,clear}}$ is strongly correlated across models with the changes in tropical longwave, clear-sky cooling (Figure 2a; $r^2 = 0.74$, $p < 0.01$), and not significantly correlated with extratropical changes in longwave, clear-sky cooling (Figure 2b; $r^2 = 0.21$, $p > 0.05$). This suggests we can parameterize the relationship between $\Delta\eta_{\text{LW,clear}}$ and its tropical component, $\Delta\langle\eta_{\text{LW,clear}}\rangle$, as:

$$\Delta\eta_{\text{LW,clear}} \approx \alpha + \beta\,\Delta\langle\eta_{\text{LW,clear}}\rangle. \tag{4}$$

The coefficients in Equation 4 are $\alpha \approx 0.01$ mm day^{-1} K^{-1} and $\beta \approx 0.35$. These values are slightly different from what one may initially expect given that the tropics cover half of the Earth ($\alpha \approx 0.006$ mm day^{-1} K^{-1}, $\beta = 0.5$), and we explain this small discrepancy in Text S2 in Supporting Information S1.

Given these observations, for the rest of the paper we will mainly focus on understanding the *tropical* contribution to $\Delta\eta_{\text{LW,clear}}$, written as $\Delta\langle\eta_{\text{LW,clear}}\rangle$, and use Equation 4 to convert this understanding to an estimate of the full $\Delta\eta_{\text{LW,clear}}$ when required.

5. A Theoretical Bridge Between SST Patterns and Radiative Cooling

We have shown that η is systematically larger in uniform warming experiments compared to abrupt-4xCO$_2$ forcing (a positive $\Delta\eta$), and that this is driven by the larger changes in longwave, clear-sky cooling $\left(\Delta\eta_{\text{LW, clear}}\right)$ under uniform warming compared to abrupt-4xCO$_2$. In this section we develop a theory which links changes in clear-sky longwave cooling to SST patterns (building off the work of JR18) as a step toward explaining the positive $\Delta\eta_{\text{LW, clear}}$.

To begin with, we note that within the boundary layer radiative cooling is largely balanced by sensible heat fluxes, and so changes in clear-sky longwave cooling ($Q_{\text{LW, clear}}$) with warming can be approximated by changes in the longwave cooling of the *free-troposphere*, the area above the boundary layer but below the tropopause (see discussion in Takahashi (2009) and O'Gorman et al. (2012)). This allows us to leverage the work of Jeevanjee and Romps (2018), who developed a simple model of changes in *free-tropospheric* radiative cooling, to understand our results.

The theory of Jeevanjee and Romps (2018) starts from the observation that free-tropospheric radiative cooling can be written as the vertical integral of the radiative flux divergence in temperature coordinates ($-\partial_T F$, where ∂_T is a

vertical derivative with respect to atmospheric temperature and F is the net upwards clear-sky radiative flux in the longwave). Mathematically, we write this as

$$Q_{\text{LW, clear}} \approx \int_{T_{\text{tp}}}^{T_B} (-\partial_{T'} F) \, dT',$$ (5)

where T_{tp} is the tropopause temperature and T_B is the temperature at the "bottom" of the free-troposphere (a level which we will make more precise in a moment).

The utility of this perspective is that it can be shown that $-\partial_T F(T)$ depends only on the *local* atmospheric temperature, T, and does not depend on the temperature at any other level. Importantly, $-\partial_T F(T)$ is insensitive to changes in surface temperature, T_s. This "T_s-invariance" arises because longwave radiative cooling is dominated by emission from optically thick water vapor lines, which occur at a fixed atmospheric temperature (this is related to "Simpson's Law," as discussed in Ingram (2010) and Jeevanjee et al. (2021)). Given that the tropopause temperature (T_{tp}) is also insensitive to surface temperature (McKim et al., 2025; Seeley et al., 2019), we can differentiate Equation 5 to find the rate of change of $Q_{\text{LW, clear}}$ with respect to changes in surface temperature:

$$\frac{dQ_{\text{LW, clear}}}{dT_s} \approx (-\partial_T F)|_B \times \frac{dT_B}{dT_s}.$$ (6)

In words, Equation 6 says that surface warming increases $Q_{\text{LW, clear}}$ by an amount proportional to the value of the flux divergence at the bottom of the free-troposphere $\left((-\partial_T F)|_B\right)$, and the derivative of temperature at the bottom of the free-troposphere with respect to surface temperature (dT_B/dT_s) (Cohen & Pincus, 2025). Physically, this can be thought of as a "deepening" of the troposphere in temperature coordinates (cf. Figure 3 of Jeevanjee and Romps (2018)), which "exposes" more of the $-\partial_T F(T)$ curve.

In its current form, Equation 6 only applies to single-columns. To extend this to tropically integrated quantities, we use T_s to denote the global-mean surface temperature and apply a tropical average ($\langle \cdot \rangle$) to both sides of Equation 6. Recalling that derivatives commute with averages, we have

$$\langle \eta_{\text{LW,clear}} \rangle \approx \left\langle (-\partial_T F)|_B \times \frac{dT_B}{dT_s} \right\rangle.$$ (7)

Where $\langle \eta_{\text{LW,clear}} \rangle \equiv \frac{d\langle Q_{\text{LW, clear}} \rangle}{dT_s}$. To simplify the right-hand side, we make the weak-temperature gradient (WTG) assumption (e.g., Sobel et al., 2001) which allows us to replace T_B with its tropical average. This eliminates the covariance between the two terms in brackets, allowing us to write Equation 7 as:
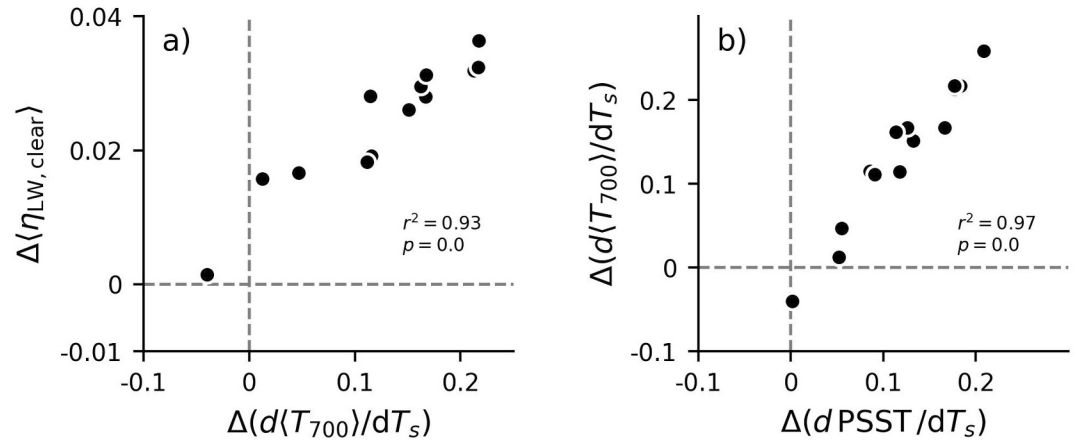
$$\langle \eta_{\text{LW,clear}} \rangle \approx \langle (-\partial_T F)|_B \rangle \times \underbrace{\frac{d\langle T_B \rangle}{dT_s}}_{\text{Pattern effect}}.$$ (8)

$\langle \eta_{\text{LW,clear}} \rangle$ is thus sensitive to changes in tropical T_B per degree of global warming $\left(\frac{d\langle T_B \rangle}{dT_s}\right)$. This term was neglected by Jeevanjee and Romps (2018) by assuming that changes in T_B are equal to changes in T_s, but is crucial for understanding the link between SST patterns and changes in radiative cooling in the tropics. This is because deep convection is the main route by which the surface and the free-troposphere "communicate" in the tropics, and SST changes in the tropics only generate a change in $\langle T_B \rangle$ if they involve warming of convective regions (Fueglistaler et al., 2015; Williams et al., 2023; Y. Zhang & Fueglistaler, 2020).

Equation 8 satisfies the goal set out in the introduction, namely to connect clear-sky radiative cooling to the SST pattern effect. A key implication of this equation is that, to the degree that models agree of the magnitude of $\langle (-\partial_T F)|_B \rangle$, we expect changes in $\langle \eta_{\text{LW,clear}} \rangle$ to scale with some measure of $\frac{d\langle T_B \rangle}{dT_s}$ across models, with the spread in $\frac{d\langle T_B \rangle}{dT_s}$ associated with different patterns of SST warming.

Applying Equation 8 to the difference between uniform and abrupt warming simulations we have

Figure 3. *Changes in tropical, longwave clear-sky cooling are strongly correlated with the amount of warming in convective regions, as predicted by theory.* (a) Scatterplot of $\Delta\langle\eta_{LW,clear}\rangle$ against $\Delta(d\langle T_{700}\rangle/dT_s)$. (b) Scatterplot of $\Delta(d\langle T_{700}\rangle/dT_s)$ against $\Delta(d\mathrm{PSST}/dT_s)$. $\Delta\langle\eta_{LW,clear}\rangle$ is in units of mm day^{-1} K^{-1}, and $\Delta(d\langle T_{700}\rangle/dT_s)$ and $\Delta(d\mathrm{PSST}/dT_s)$ are in units of K K^{-1}.

$$\Delta\langle\eta_{\text{LW,clear}}\rangle \approx \langle-\partial_T F\rangle|_B \times \Delta\left(\frac{d\langle T_B\rangle}{dT_s}\right), \tag{9}$$
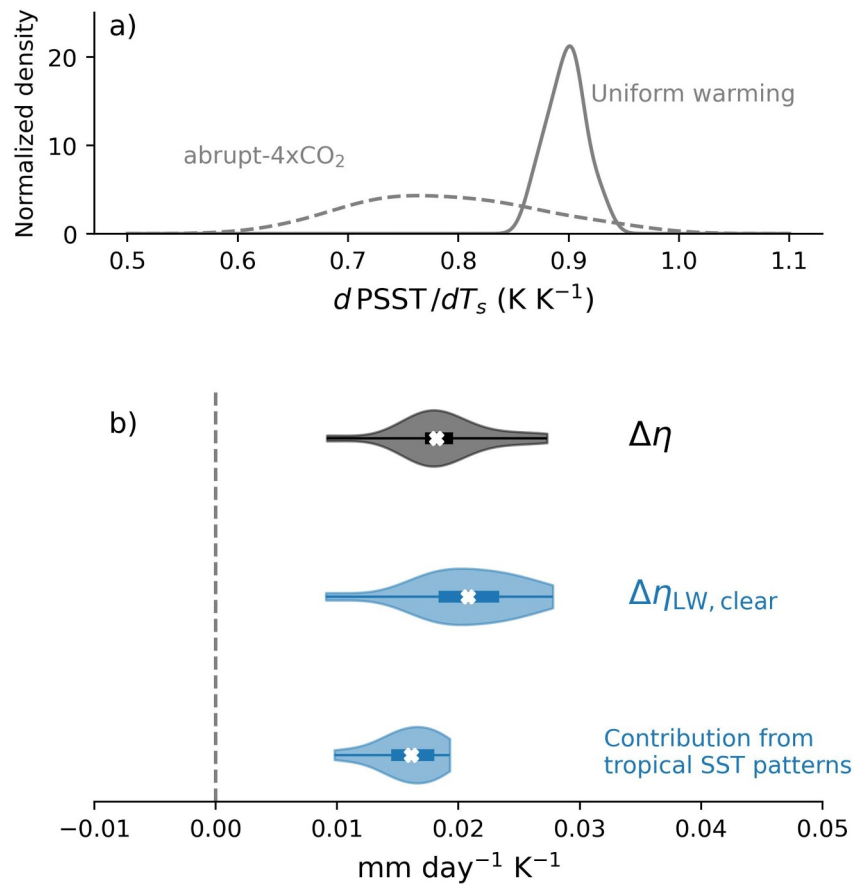
where Δ is the difference between a quantity calculated in uniform warming and abrupt-4xCO$_2$ simulations, and we have assumed that $\Delta\langle-\partial_T F\rangle|_B = 0$.

To test Equation 9 we must find the lowest free-tropospheric pressure level where the WTG approximation holds, which is where we will evaluate $\langle T_B\rangle$. A spatial coherence analysis of de-seasonalized monthly, tropical temperatures from ERA5 (Hersbach et al., 2020) suggests that this level is at around 700 hPa (Figure S3 in Supporting Information S1) so we take $T_B = T_{700}$, but our conclusions are unaffected if we use other nearby pressure levels. In Figure 3a we scatter $\Delta\langle\eta_{LW,clear}\rangle$ against $\Delta\left(\frac{d\langle T_{700}\rangle}{dT_s}\right)$ for each of the CMIP models. There is a strong, positive correlation between these two variables ($r^2 = 0.93$). Physically, this is saying that if a model has a large difference in $\frac{d\langle T_{700}\rangle}{dT_s}$ between its uniform warming and abrupt-4xCO$_2$ experiments, then it will also have a large difference in the change in tropical, longwave clear-sky cooling per degree of global-warming, in line with Equation 9.

The intercept in Figure 3a is slightly positive due to increased CO$_2$ levels in abrupt-4xCO$_2$ experiments compared to the AMIP runs, which somewhat mute the hydrological sensitivity even in the absence of SST pattern changes (Cohen & Pincus, 2025). The slope of the linear relationship in Figure 3a can also be interpreted as the multi-model mean value of $\langle-\partial_T F\rangle|_B$. Converting to energy units, we find that the slope of the data implies a multi-model mean value of ≈ 3 W m^{-2} K^{-1}, which compares reasonably well with the $\langle-\partial_T F\rangle|_{700} \approx 3$–$4$ W m^{-2} K^{-1} range of values diagnosed by JR18 using cloud-resolving simulations of tropical convection. This agreement gives us confidence that the "tropospheric deepening" perspective is useful for explaining $\Delta\langle\eta_{LW,clear}\rangle$.

Equation 9 is able to explain differences in tropical, clear-sky radiative cooling in terms of differences in $d\langle T_{700}\rangle/dT_s$, but now we would like to better understand what drives the spread in $\Delta(d\langle T_{700}\rangle/dT_s)$ across models. Physically, the temperature of the tropical free-troposphere is set by SSTs in regions of deep convection because deep convection is the primary way in which the surface and the free-troposphere "communicate" in the tropics (Emanuel, 2007; Emanuel et al., 1994; Fueglistaler et al., 2015; Sobel et al., 2001; Williams et al., 2023). To quantify the SST in regions of tropical deep convection, we use the tropical, precipitation-weighted SST (termed PSST) introduced by Fueglistaler et al. (2015). PSST is calculated as $\mathrm{PSST} = \langle P \cdot SST\rangle/\langle P\rangle$, where P is the precipitation and $\langle\cdot\rangle$ again denotes an area-weighted tropical average. PSST more strongly weights SST changes that occur in regions of deep convection with high precipitation, and thus captures the physical links between free-tropospheric temperatures, deep convection, and SSTs. As we can see in Figure 3b, models which have a larger $d\langle T_{700}\rangle/dT_s$ in uniform warming than abrupt-4xCO$_2$ also exhibit greater SST warming in regions of

Figure 4. *Differences in sea-surface temperature (SST) warming in convective regions largely account for differences in hydrological sensitivity.* (a) Kernel density estimates of changes in tropical PSST per degree of global warming in abrupt-4xCO$_2$ and uniform warming runs. The kernel density estimates are computed using the `gaussian_kde` function from SciPy (Virtanen et al., 2020). (b) The difference in hydrological sensitivity between uniform warming and abrupt-4xCO$_2$ simulations, the contribution from clear-sky longwave radiative cooling ($\Delta\eta_{\text{LW,clear}}$), and an estimate of the contribution to $\Delta\eta_{\text{LW,clear}}$ from differences in tropical SST warming patterns (based on Equations 10 and 4).

tropical deep convection ($d\text{PSST}/dT_s$) under uniform warming than abrupt-4xCO$_2$ scenarios. The regression slope in Figure 3b is about 1.4, consistent with expectations from a moist adiabat (e.g., Merlis et al., 2024).

6. Tropical SST Warming Patterns Drive $\Delta\eta$ Across Models

Now that we have developed a theory which links changes in tropical clear-sky longwave cooling to patterns of SST change, we return to the question of why $\eta_{\text{LW, clear}}$ is systematically larger in uniform warming experiments than coupled experiments with abrupt-4xCO$_2$ forcing.

In Figure 4a, we show Gaussian distributions of $d\text{PSST}/dT_s$ in the ensemble of uniform warming and abrupt-4xCO$_2$ simulations. In abrupt-4xCO$_2$ simulations, $d\text{PSST}/dT_s$ is much more variable than in the uniform warming simulations, in line with the fact that the SST changes are identical in the uniform warming simulations, but model-dependent in the abrupt-4xCO$_2$ simulations. The salient feature of Figure 4a is that $d\text{PSST}/dT_s$ tends to be larger in uniform warming simulations than in abrupt-4xCO$_2$ simulations, reflecting the fact that warming in coupled models tends to be focused in the eastern tropical Pacific (sometimes referred to as being "El Niño-like") where there is less convection and rainfall than in the western tropical Pacific. Meanwhile, uniform warming simulations warm SSTs over the deeply convecting regions of the tropics as much as the rest of the globe, thus generating a larger $d\text{PSST}/dT_s$. Note that it is not circular to explain differences in hydrological sensitivity using PSST because PSST only encodes information on the *pattern* of precipitation and not its magnitude.

To get a back-of-the-envelope estimate of how big an effect these inter-scenario differences in $d\mathrm{PSST}/dT_s$ have on tropical, longwave clear-sky cooling we can use Equation 9 and replace $\langle T_{700} \rangle$ with PSST,

$$\Delta\langle \eta_{\mathrm{LW,clear}} \rangle \approx \langle -\partial_T F \rangle|_B \times \Delta\left(\frac{d\mathrm{PSST}}{dT_s}\right). \tag{10}$$

The average $d\mathrm{PSST}/dT_s$ under uniform warming is ≈ 0.9 K K^{-1} compared to ≈ 0.78 K K^{-1} under abrupt-4xCO$_2$ forcing. Using these values in Equation 10 along with a characteristic value of $\langle -\partial_T F \rangle|_B \approx 3$ W m^{-2} K^{-1} $\approx$ 0.1 mm day^{-1} K^{-1} yields a rough estimate of the change in tropical, longwave clear-sky cooling between uniform and abrupt warming scenarios of ≈ 0.01 mm day^{-1} K^{-1}. To convert this tropical estimate into an estimate of $\Delta\eta_{\mathrm{LW,clear}}$, we use Equation 4 (Figure 2a). This yields an estimate of $\Delta\eta_{\mathrm{LW,clear}} \approx 0.016$ mm day^{-1} K^{-1}, in good agreement with the average $\Delta\eta_{\mathrm{LW,clear}}$ across the CMIP models (Figure 4b).

We can use this procedure, based on Equations 10 and 4, to estimate $\Delta\eta_{\mathrm{LW,clear}}$ using $\Delta(d\mathrm{PSST}/dT_s)$ for each of the CMIP models, and the distribution of these estimates is also shown in Figure 4b. This estimate relies only on $d\mathrm{PSST}/dT_s$, and a small, empirical correction (Equation 4) which relates tropical changes to global changes in longwave clear-sky cooling. The resulting distribution gives a reasonable estimate of $\Delta\eta_{\mathrm{LW,clear}}$ across models, although slightly underestimates the high-end of changes. However, as we stated in Section 3, our goal here is to explain the multi-model mean value of $\Delta\eta$, which is closely approximated by our estimate. We note that the discrepancy between our median PSST estimate and the true $\Delta\eta_{\mathrm{LW,clear}}$ is similar to our approximate estimate of the magnitude of the CO$_2$ masking effect (Figure S1 in Supporting Information S1), which suggests that enhanced CO$_2$ masking under abrupt-4xCO$_2$ forcing may also play a role in setting $\Delta\eta$ (Cohen & Pincus, 2025).

7. Conclusions

Our main results are:

- Hydrological sensitivity, η, is systematically larger in uniform warming than abrupt-4xCO$_2$ scenarios (Figure 1a), associated with larger increases in longwave clear-sky radiative cooling in uniform warming runs (Figure 1b).
- These differences in longwave, clear-sky cooling are driven by changes in longwave, clear-sky cooling in the tropics (Figure 2a).
- These changes in longwave, clear-sky cooling are related to different SST warming rates in regions of tropical deep convection.
- Existing theories for radiative cooling and hydrological sensitivity can be extended to incorporate the SST pattern effect (Equations 10 and 4).

This new understanding of the links between SST patterns and radiative cooling, encapsulated in Equation 10, can be used to understand some of the intriguing results we referenced in the introduction. As a reminder, both Zhao and Knutson (2024) and S. Zhang et al. (2023) previously found that η was different depending on the pattern of SST warming, but neither provided a compelling physical argument for why this should be the case. Zhao and Knutson (2024) found that η was larger when the observed pattern of SST warming was imposed in a model compared to when the pattern was taken from the historical run of a coupled climate model. This can be understood in our framework as being due to a stronger $d\mathrm{PSST}/dT_s$ in response to the observed SST pattern, which warms more strongly in the Western tropical Pacific (a convective region) than the Eastern tropical Pacific (a largely non-convective region). Similarly, S. Zhang et al. (2023) noted that when "patches" of SST warming were imposed in the Western tropical Pacific, the resulting η was larger. Hence, differential warming in regions of tropical convection, and the subsequently different amounts of "tropospheric deepening," can explain different values of η seen in previous literature.

Our perspective also explains why Fläschner et al. (2016) concluded, erroneously, that patterned SST warming is *not* the reason for higher mean η in uniform warming simulations. This conclusion was based off the fact that η estimated from AMIP-future4K simulations (which exhibit patterned SST warming) is similar to η_{uniform}. However, the warming pattern in AMIP-future4K simulations differs markedly from the abrupt4xCO$_2$ warming trend in CMIP models (Qin et al., 2022; S. Zhang et al., 2023) and exhibits a tropical warming pattern which is in

fact quite uniform (Voigt et al., 2024). Although AMIP-future4K simulations exhibit patterned warming, their warming in regions of tropical convection is similar to uniform warming scenarios.

Our work is able to explain differences in η so long as these differences are driven by clear-sky longwave radiative cooling, which we can link to tropical SST patterns. Previous work by S. Zhang et al. (2023) argued that half of the *inter-model* spread in η under abrupt-4xCO$_2$ forcing can be ascribed to differences in SST patterns. However, as we show in Figures S4 and S5 in Supporting Information S1, there is no significant correlation between η and $\eta_{LW,clear}$ across CMIP5/6 models under abrupt-4xCO$_2$ forcing. Hence, the mechanisms we identify here linking SST patterns to radiative cooling are not able to explain the inter-model spread in η under abrupt-4xCO$_2$ forcing. Thus if SST patterns do contribute to the inter-model spread in η under abrupt-4xCO$_2$ it must be through other mechanisms, such as cloud feedbacks.

Kao and Pendergrass (2024) recently found that the value of η depended in abrupt-4xCO$_2$ simulations depended on the *timescale* over which it was calculated. That is, whether the regressions were taken over years 1–20, 21–150 or 151–1,000 of LongRunMIP simulations (Rugenstein et al., 2019). This behavior is similar to the timescale-dependence of the feedback parameter, λ, in abrupt-4xCO$_2$ simulations, which has been linked to changes in the pattern of warming over time (Dong et al., 2020). Future work could examine whether the timescale-dependence of η is due to changes in longwave cooling and if so, whether these changes are due to a timescale-dependence of the amount of warming in tropical convective regions.

Conflict of Interest

The authors declare no conflicts of interest relevant to this study.

Data Availability Statement

Data supporting the conclusions in this article are archived at Williams (2025).

References

Allen, M. R., & Ingram, W. J. (2002). Constraints on future changes in climate and the hydrologic cycle. *Nature*, *419*(6903), 228–232. https://doi.org/10.1038/nature01092

Cohen, S., & Pincus, R. (2025). A spectroscopic theory for how mean rainfall changes with surface temperature. *Science Advances*, *11*(19), eadv6191. https://doi.org/10.1126/sciadv.adv6191

DeAngelis, A. M., Qu, X., Zelinka, M. D., & Hall, A. (2015). An observational radiative constraint on hydrologic cycle intensification. *Nature*, *528*(7581), 249–253. https://doi.org/10.1038/nature15770

Dong, Y., Armour, K. C., Zelinka, M. D., Proistosescu, C., Battisti, D. S., Zhou, C., & Andrews, T. (2020). Intermodel spread in the pattern effect and its contribution to climate sensitivity in CMIP5 and CMIP6 models. *Journal of Climate*, *33*(18), 7755–7775. https://doi.org/10.1175/jcli-d-19-1011.1

Emanuel, K. A. (2007). Quasi-equilibrium dynamics of the tropical atmosphere. *The Global Circulation of the Atmosphere*, *186*, 218. https://doi.org/10.1515/9780691236919-009

Emanuel, K. A., David Neelin, J., & Bretherton, C. S. (1994). On large-scale circulations in convecting atmospheres. *Quarterly Journal of the Royal Meteorological Society*, *120*(519), 1111–1143. https://doi.org/10.1002/qj.49712051902

Fläschner, D., Mauritsen, T., & Stevens, B. (2016). Understanding the intermodel spread in global-mean hydrological sensitivity. *Journal of Climate*, *29*(2), 801–817. https://doi.org/10.1175/JCLI-D-15-0351.1

Fueglistaler, S., Radley, C., & Held, I. M. (2015). The distribution of precipitation and the spread in tropical upper tropospheric temperature trends in CMIP5/AMIP simulations. *Geophysical Research Letters*, *42*(14), 6000–6007. https://doi.org/10.1002/2015gl064966

Hersbach, H., Bell, B., Berrisford, P., Hirahara, S., Horányi, A., Muñoz-Sabater, J., et al. (2020). The ERA5 global reanalysis. *Quarterly Journal of the Royal Meteorological Society*, *146*(730), 1999–2049. https://doi.org/10.1002/qj.3803

Ingram, W. (2010). A very simple model for the water vapour feedback on climate change. *Quarterly Journal of the Royal Meteorological Society: A Journal of the Atmospheric Sciences, Applied Meteorology and Physical Oceanography*, *136*(646), 30–40. https://doi.org/10.1002/qj.546

Jeevanjee, N., Koll, D. D., & Lutsko, N. (2021). "Simpson's law" and the spectral cancellation of climate feedbacks. *Geophysical Research Letters*, *48*(14), e2021GL093699. https://doi.org/10.1029/2021gl093699

Jeevanjee, N., & Romps, D. M. (2018). Mean precipitation change from a deepening troposphere. *Proceedings of the National Academy of Sciences of the United States of America*, *115*(45), 11465–11470. https://doi.org/10.1073/pnas.1720683115

Kao, K., & Pendergrass, A. G. (2024). Timescale dependence of the precipitation response to CO$_2$-induced warming in millennial-length climate simulations. *Geophysical Research Letters*, *51*(21), e2024GL111609. https://doi.org/10.1029/2024gl111609

Manabe, S., & Wetherald, R. T. (1975). The effects of doubling the CO$_2$ concentration on the climate of a general circulation model. *Journal of the Atmospheric Sciences*, *32*(1), 3–15. https://doi.org/10.1175/1520-0469(1975)032<0003:teodtc>2.0.co;2

McKim, B. A., Jeevanjee, N., Vallis, G. K., & Lewis, N. T. (2025). Water vapor spectroscopy and thermodynamics constrain Earth's tropopause temperature. *AGU Advances*, *6*(2), e2024AV001206. https://doi.org/10.1029/2024av001206

Merlis, T. M., Guendelman, I., Cheng, K.-Y., Harris, L., Chen, Y.-T., Bretherton, C. S., et al. (2024). The vertical structure of tropical temperature change in global storm-resolving model simulations of climate change. *Geophysical Research Letters*, *51*(23), e2024GL111549. https://doi.org/10.1029/2024gl111549

Mitchell, J., Wilson, C., & Cunnington, W. (1987). On CO_2 climate sensitivity and model dependence of results. *Quarterly Journal of the Royal Meteorological Society*, *113*(475), 293–322. https://doi.org/10.1002/qj.49711347517

O'Gorman, P. A., Allan, R. P., Byrne, M. P., & Previdi, M. (2012). Energetic constraints on precipitation under climate change. *Surveys in Geophysics*, *33*(3–4), 585–608. https://doi.org/10.1007/s10712-011-9159-6

Pendergrass, A. G., & Hartmann, D. L. (2014). The atmospheric energy constraint on global-mean precipitation change. *Journal of Climate*, *27*(2), 757–768. https://doi.org/10.1175/JCLI-D-13-00163.1

Qin, Y., Zelinka, M. D., & Klein, S. A. (2022). On the correspondence between atmosphere-only and coupled simulations for radiative feedbacks and forcing from CO_2. *Journal of Geophysical Research: Atmospheres*, *127*(3), e2021JD035460. https://doi.org/10.1029/2021jd035460

Rugenstein, M., Bloch-Johnson, J., Abe-Ouchi, A., Andrews, T., Beyerle, U., Cao, L., et al. (2019). LONGRUNMIP: Motivation and design for a large collection of millennial-length AOGCM simulations. *Bulletin of the American Meteorological Society*, *100*(12), 2551–2570. https://doi.org/10.1175/bams-d-19-0068.1

Seeley, J. T., Jeevanjee, N., & Romps, D. M. (2019). FAT or FiTT: Are anvil clouds or the tropopause temperature invariant? *Geophysical Research Letters*, *46*(3), 1842–1850. https://doi.org/10.1029/2018gl080096

Sobel, A. H., Nilsson, J., & Polvani, L. M. (2001). The weak temperature gradient approximation and balanced tropical moisture waves. *Journal of the Atmospheric Sciences*, *58*(23), 3650–3665. https://doi.org/10.1175/1520-0469(2001)058⟨3650:TWTGAA⟩2.0.CO;2

Takahashi, K. (2009). Radiative constraints on the hydrological cycle in an idealized radiative–convective equilibrium model. *Journal of the Atmospheric Sciences*, *66*(1), 77–91. https://doi.org/10.1175/2008jas2797.1

Virtanen, P., Gommers, R., Oliphant, T. E., Haberland, M., Reddy, T., Cournapeau, D., et al. (2020). Scipy 1.0: Fundamental algorithms for scientific computing in python. *Nature Methods*, *17*(3), 261–272. https://doi.org/10.1038/s41592-019-0686-2

Voigt, A., North, S., Gasparini, B., & Ham, S.-H. (2024). Atmospheric cloud-radiative heating in CMIP6 and observations and its response to surface warming. *Atmospheric Chemistry and Physics*, *24*(17), 9749–9775. https://doi.org/10.5194/acp-24-9749-2024

Williams, A. I. L. (2025). Supporting data for "sea-surface temperature patterns, radiative cooling, and hydrological sensitivity" [Dataset]. *Zenodo*. https://doi.org/10.5281/zenodo.17127165

Williams, A. I. L., Jeevanjee, N., & Bloch-Johnson, J. (2023). Circus tents, convective thresholds, and the non-linear climate response to tropical SSTs. *Geophysical Research Letters*, *50*(6), e2022GL101499. https://doi.org/10.1029/2022gl101499

Zhang, S., Stier, P., Dagan, G., Zhou, C., & Wang, M. (2023). Sea surface warming patterns drive hydrological sensitivity uncertainties. *Nature Climate Change*, *13*(6), 545–553. https://doi.org/10.1038/s41558-023-01678-5

Zhang, Y., & Fueglistaler, S. (2020). How tropical convection couples high moist static energy over land and ocean. *Geophysical Research Letters*, *47*(2), e2019GL086387. https://doi.org/10.1029/2019GL086387

Zhao, M., & Knutson, T. (2024). Crucial role of sea surface temperature warming patterns in near-term high-impact weather and climate projection. *npj Climate and Atmospheric Science*, *7*(1), 130. https://doi.org/10.1038/s41612-024-00681-7